ORNL/CP-99118

CONF-980657--



# Atom probe field-ion microscopy investigation of nickel base superalloy welds[†]

S. S. Babu — Oak Ridge National Laboratory, Oak Ridge, TN 37831, USA
S. A. David — Oak Ridge National Laboratory, Oak Ridge, TN 37831, USA
J. M. Vitek — Oak Ridge National Laboratory, Oak Ridge, TN 37831, USA
M. K. Miller — Oak Ridge National Laboratory, Oak Ridge, TN 37831, USA



[†] The research was sponsored by the Division of Materials Sciences, U.S. Department of Energy, under contract DE-AC05-96OR22464 with Lockheed Martin Energy Research Corporation.

# DISCLAIMER

## Introduction

Welding of single crystal and directionally solidified nickel base superalloys is gaining increasing importance because of the need for repair welding and rebuilding of failed and eroded components. The microstructure in the weld fusion zone and heat-affected-zone (HAZ) that result from rapid temperature excursions control the weldability and the service performance of the welded components. Therefore, recent work has concentrated on the weldability issues[1] and microstructure development in single-crystal welds.[2] These studies have shown complex interactions between weld pool shape, crystallographic parameters, solidification features and solid-state phase transformations and microstructure evolution. In general, the weld microstructure evolution sequence involves formation of $\gamma$ dendrite from liquid and epitaxial solidification of $\gamma$ grains in the HAZ adjacent to fusion line, formation of eutectics along the dendritic boundaries, and precipitation of $\gamma'$ phases within the $\gamma$ dendrites. The present study pertains to the precipitation of the $\gamma'$ phase and elemental partitioning between $\gamma$ and $\gamma'$ phase.

Precipitation of $\gamma'$ phase in nickel base superalloys involves homogeneous nucleation and growth. However, the precipitation during rapid continuous weld cooling may lead to nucleation at large undercoolings, non-equilibrium partitioning and interfacial segregation between $\gamma$ and $\gamma'$ phases. This work reviews the fine-scale $\gamma$-$\gamma'$ partitioning characteristics in PWA-1480 and CMSX-4 single crystal welds measured by atom probe field-ion microscopy.[3,4] Moreover, the precipitation of $\gamma'$ under continuous cooling conditions were investigated in CM247DS alloy using a thermo-mechanical simulator. The above work will aid in understanding the microstructure development and its effect on the weldability and properties.

## Experimentation

**Alloys:** Single crystal PWA-1480 and CMSX-4 alloys and directionally solidified CM247DS alloys were investigated in this work. The compositions are given in Table 1. The alloys were examined in the as-cast condition.

Table. 1 Composition of alloys studied in wt.%.

| Alloy | Al | Cr | Ti | Co | Ta | W | Ni |
|---|---|---|---|---|---|---|---|
| PWA-1480 | 5.0 | 10.0 | 1.5 | 5.0 | 12.0 | 4.0 | Bal. |
| CMSX-4* | 5.5 | 6.5 | 1.0 | 7.0 | 7.0 | 6.5 | Bal. |
| CM247DS | 5.5 | 8.0 | 0.8 | 9.0 | 3.2 | 9.5 | Bal. |

*2.9 wt.% Re is also present in CMSX-4 alloys.

**Welding Procedure:** Autogenous full-penetration electron beam welds were made on 2-3 mm thick discs extracted from cast single crystals of PWA-1480 alloy. The welding parameters were as follows: accelerating voltage, 100-125 kV; welding current, 7.5 to 10 mA; and welding speed, 4.2 $\times 10^{-3}$ m $s^{-1}$. The preheat temperature was 500 °C. Autogenous full-penetration pulsed-laser welds were made on 2-3 mm thick sheets of CMSX-4 alloy machined from single crystals. There was no preheating before welding. The welding parameters were as follows: average laser power ~ 400 W, laser pulse rate 40 $s^{-1}$, and welding speed: $2.1 \times 10^{-3}$ and $1.27 \times 10^{-2}$ m $s^{-1}$.

**Characterization:** Detailed microstructural analysis was performed using optical and electron microscopy techniques. In addition, an atom probe field-ion microscope was used to characterize the partitioning at the $\gamma$–$\gamma'$ interfaces in the as-welded condition. The samples were imaged at a temperature range of 50 to 60 K and analyzed with a residual neon gas pressure of $3 \times 10^{-7}$ Pa and a pulse fraction of 20% in the atom probe.

**Controlled Phase Transformation Study:** The precipitation kinetics of γ′ in the CM247DS alloy was studied using Gleeble Thermo-mechanical Simulator. In this investigation, rod samples (6.3 mm diameter) were machined from the castings. These samples were solutionized at 1300 °C for 5 minutes and were cooled at different rates (1, 10 and 75 $°Cs^{-1}$). The relative radius changes of samples during cooling were measured with a dilatometer. For comparison, pure nickel samples were also investigated.

**Thermodynamic and Kinetic Calculations:** Thermodynamic calculations on the elemental partitioning of the nickel base superalloys were performed with ThermoCalc.[5] Equilibrium conditions were computed using the Ni-Database, a thermodynamic database for calculation of phase equilibria in multi-component alloys.[6] The effect of Ta and W are not considered in the calculations. Growth of γ′ phase in γ phase was calculated for the Ni- 20 at.% Al - 5 at.% Cr alloy system with diffusion controlled growth software (DicTra).[7] Since the diffusion controlled growth software does not have the data on diffusivity of elements in γ′ phase, the diffusion in the γ′ phase is not considered. Therefore, the calculations consider only diffusion of Cr, Al, and Ni in the γ phase. The calculations considered 1, 10, and 75 $°Cs^{-1}$ cooling rates. In these calculations, the spacing between two γ′ precipitates was taken as 2 μm. Note that the spacing will be different for different number densities of γ′ precipitates and this will be considered in the future work.

## Results and Discussion

**PWA-1480 Electron Beam Welds:** Optical microscopy of welds indicated a dendritic solidification. Transmission electron microscopy (Fig. 1) revealed large γ′ phase interlaced with γ phase along the inter-dendritic boundary. Their morphology suggests that this is the product of eutectic decomposition of liquid during the final stages of solidification (L -> γ + γ′). The microstructure also revealed cuboidal γ′ precipitates within the core of the γ dendrites. The size of these precipitates varied from 0.05 to 0.5 μm.

The formation of eutectic γ′ due to solidification partitioning, as well as the precipitation of γ′ was supported by thermodynamic calculations with ThermoCalc software.[5] Thermodynamic calculations also indicated that the partitioning characteristics between γ and γ′ phases vary as a function of growth temperature (Fig. 2).[8] Therefore, it is important to measure the partitioning characteristics experimentally.

The atom probe field-ion microscope was used to measure the partitioning between γ and γ′ phases. A field-ion image of a γ-γ′ interface is shown in Fig. 3 (*a*). Typical concentration profiles of Cr and Al are shown in Fig. 3 (*b*). Other elemental concentration profiles can be found elsewhere.[3]

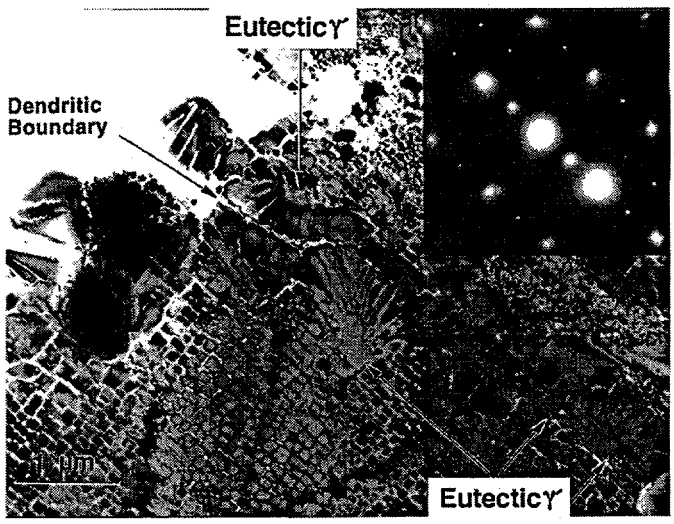


Fig. 1. Transmission electron micrograph of PWA-1480 electron beam weld. The inset is the electron diffraction showing the presence of $L1_2$ ordered γ′ phase.

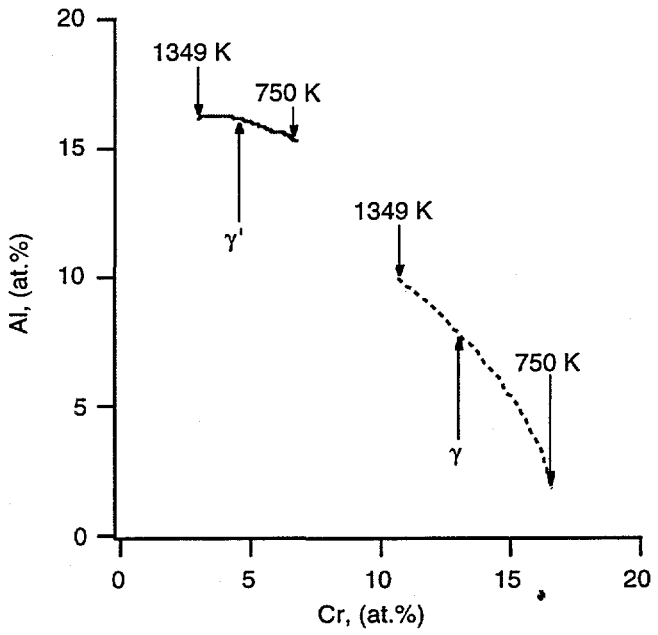


Fig. 2. Calculated equilibrium concentration of Cr and Al in γ and γ′ phases over the 700-1349 K temperature range for a nickel base superalloy (Ni - 5 wt.% Al - 10.0 wt.% Cr - 1.5 wt.% Ti - 5.0 wt.% Co).

The compositions of γ and γ′ were found to be similar to the values measured from base-metal.[9] The composition profile showed the absence of segregation at the interface and also suggested that the concentration gradients within γ and γ′ phases were not significant. This showed that in spite of continuous cooling conditions, the

decomposition of γ to γ′ appears to have occurred in a fashion similar to that after standard heat treatments. This must be attributed to relatively slow cooling in the electron beam welds. In this context, one needs to consider the precipitation kinetics of γ′ during continuous cooling conditions, which will be dealt with in a later section.

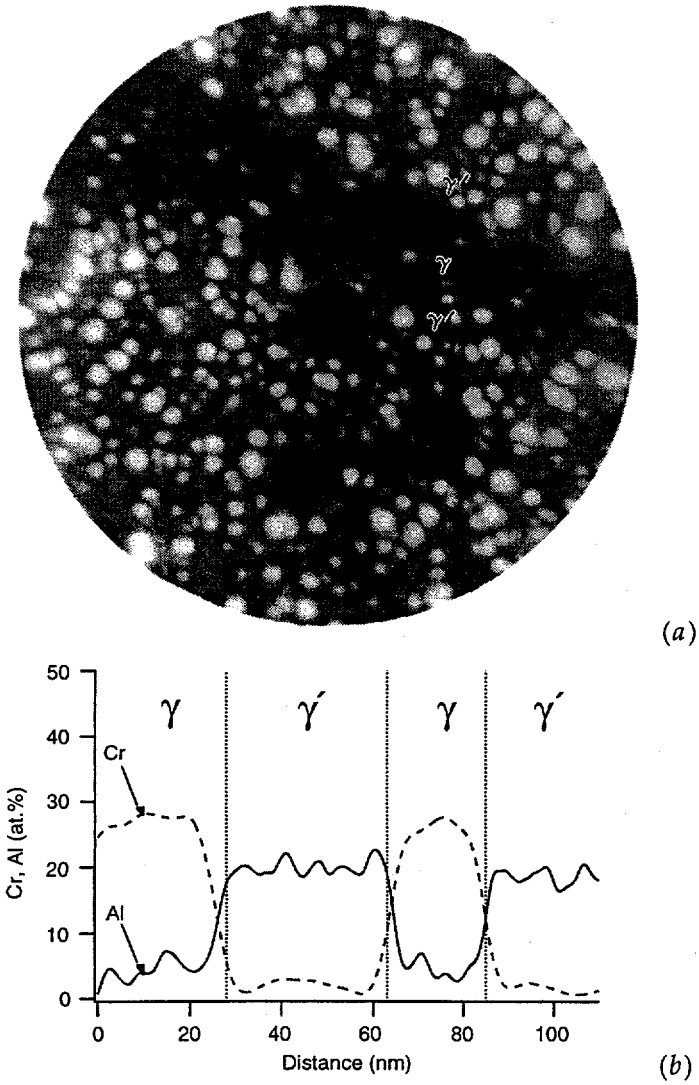


Fig. 3 (*a*) Field-ion micrograph of γ/γ′ interface in a PWA-1480 electron beam weld. (*b*) APFIM concentration profile of aluminum and chromium within γ or γ′ phases

**CMSX-4 Pulsed Laser Welds:** Optical microstructure of welds indicated a very fine cellular dendritic structure. Moreover, the transmission electron micrographs (Fig. 4) revealed negligible amounts of eutectic γ-γ′ along the dendritic boundaries. Thermodynamic calculations indicated that CMSX-4 alloys also should exhibit eutectic γ′ formation. The absence of eutectic γ′ was attributed to rapid weld cooling conditions in the weld. The absence of eutectic γ′ phase may have significant effect on weldability. The diffusion controlled growth calculations supported the hypothesis that rapid weld cooling may lead to solidification without the formation of eutectic γ′.[10]

The most interesting observation was the presence of γ′ precipitates within the dendrites and that they were finer (10 to 50 nm) than the γ′ precipitates found in PWA-1480 EB welds. The shapes of these precipitates were found to be irregular in comparison to regular cuboidal shaped ones in the base metal. It is speculated that the size and morphology could be related to nucleation under rapid cooling conditions and nonequilibrium elemental partitioning between γ and γ′ phases, respectively, as discussed below.

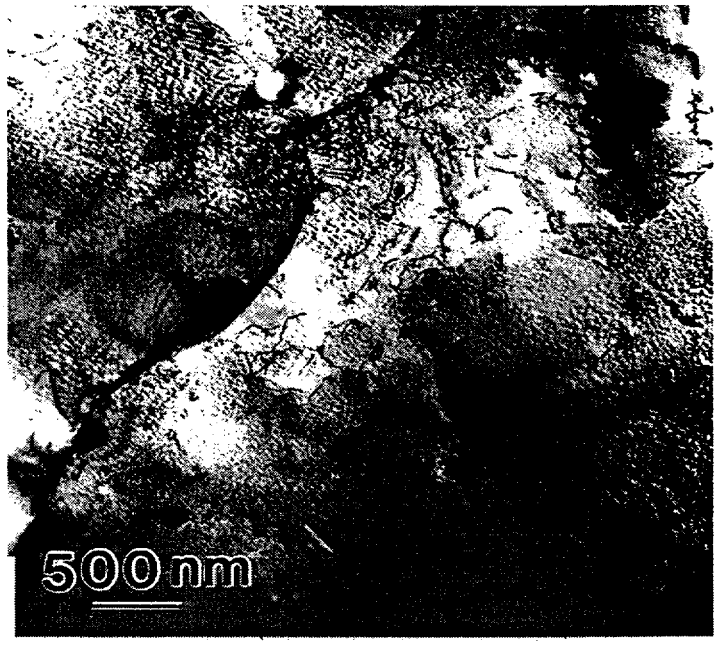


Fig. 4 Transmission electron micrograph of CMSX-4 weld zone. Negligible amounts of eutectic γ′ were observed.

The elemental partitioning in these welds was measured using atom probe field ion microscopy (FIM). The FIM image of the γ-γ′ interface is shown in Fig. 5 (*a*). The atom probe composition profile across the interface is shown in Fig. 5 (*b*). The concentration profiles showed extensive gradients of aluminum and chromium concentration in γ phase and the composition of the γ and γ′ phases were different from that of the base metal.[11] In addition, the lattice misfit of γ and γ′, based on the measured interface concentrations, was found to be positive compared to a negative value for that of the base metal.[4] This may lead to lattice strains that in turn may induce changes in the γ′ precipitate morphology.

In the results presented above, an important observation was the difference in size of the γ′ precipitates within the γ dendrites. In PWA-1480 welds, coarse γ′ precipitates were observed compared to finer γ′ phase in CMSX-4 pulsed laser welds. This difference in

the size may be related to the difference in nucleation conditions in the solid state during weld cooling. The nucleation rates are related to undercooling and the chemical driving force for nucleation. Preliminary calculations indicated that the difference in chemical composition between PWA-1480 and CMSX-4 might not lead to large differences in the driving force for nucleation at a given temperature. However, rapid weld cooling in the case of CMSX-4 pulsed laser welds may lead to nucleation at large undercoolings, in comparison to small undercoolings for electron beam welds.*

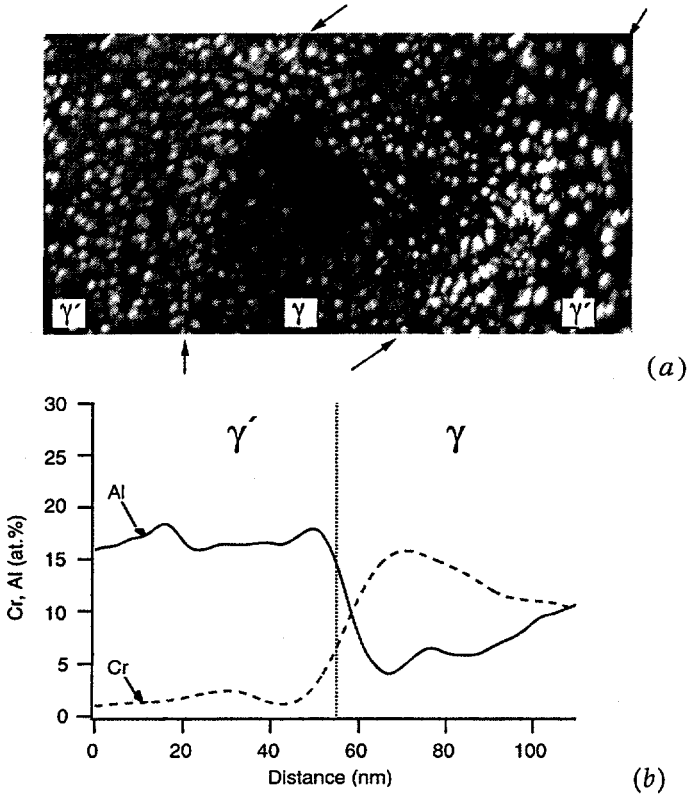


Fig. 5 (a) Field-ion micrograph of γ-γ′ interface in a CMSX-4 pulsed laser beam weld. (*b*) APFIM concentration profiles of aluminum and chromium showing large concentration gradients within the γ phase.

**CM247DS Controlled Phase Transformation Study:** To avoid ambiguity in relating the nucleation rate to either the chemical composition difference or the cooling rate difference, controlled phase transformation experiments at different cooling rates were performed on a CM247DS alloy, whose composition is similar to that of CMSX-4.

The differential thermal analysis (Fig. 6) on CM247DS alloy showed the γ′ solvus temperature range to be 1018 to 1279 °C.[8] The solvus temperature region was identified from the slope change in the differential thermal analysis curve. Therefore, CM247DS samples were solutionized at 1300 °C for 5 minutes. After the solutionizing treatment, the samples were cooled under controlled conditions. The relative radius change of the samples was monitored continuously using dilatometry.

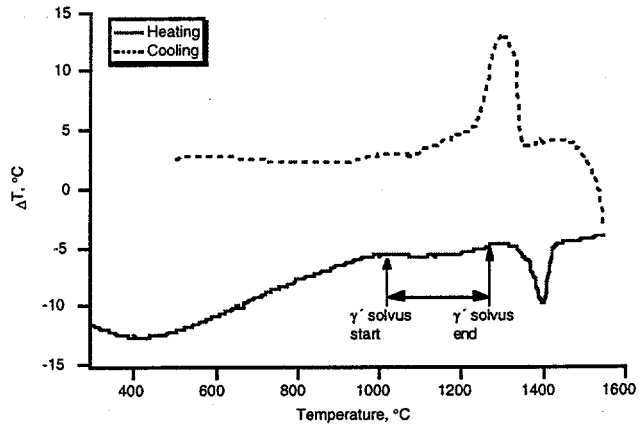


Fig. 6 Differential thermal analysis results from CM247DS material during heating and cooling.

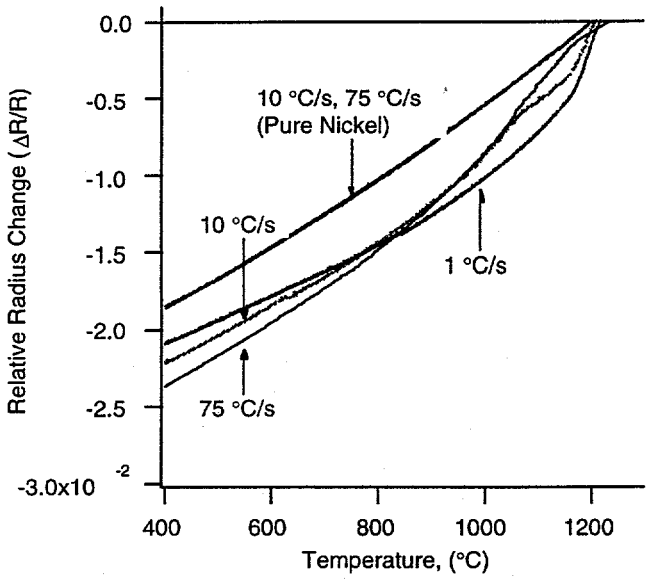


Fig. 7 Measured relative radius change with temperature of CM247DS material for different cooling rates.

In general, the dilatometry measurements are sensitive to volume change and the coefficient of thermal expansion changes due to phase transformations.[12] The results from CM247DS alloys and pure nickel samples (Fig. 7) show distinct differences in relative radius change with temperature for three different cooling rates, which was not observed in the pure nickel. This change may be related to the γ′ nucleation and growth kinetics. However, quantitative evaluation of dilatometry changes in terms of volume fraction of γ′ is

*It is important to note that EB welds were made with preheat of 500 °C to avoid weld cracking. This high preheat temperature will lead to slow weld cooling rates.

beyond the scope of the present paper. The change in the $\gamma'$ precipitation kinetics needs to be supported by microstructural characterization.

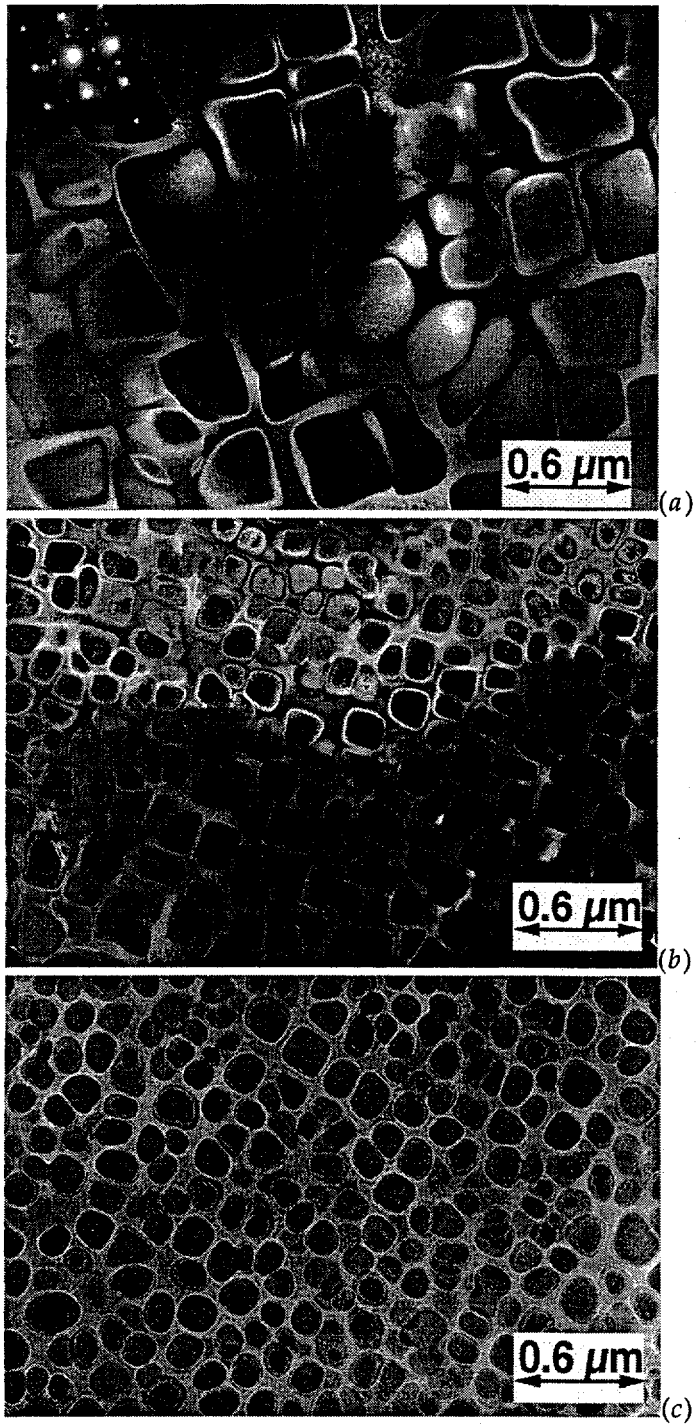


Fig. 8 Transmission electron micrograph of CM247DS material cooled at (*a*) 1 °Cs$^{-1}$, the inset shows the electron diffraction pattern indicating the presence of $L1_2$ ordered $\gamma'$ phases in the microstructure; (*b*) 10 °Cs$^{-1}$ and (*c*) 75 °Cs$^{-1}$ after solutionizing at 1300 °C for 5 min.

Transmission electron micrographs (Fig. 8) show that the number density of $\gamma'$ phase is higher in the samples cooled at 10 and 75 °Cs$^{-1}$ compared to 1 °Cs$^{-1}$. The results suggest that nucleation of $\gamma'$ phase occurred at large undercoolings and therefore large nucleation rates. This, in turn, leads to an increased number density of $\gamma'$ precipitates. This result is in agreement with the microstructure in PWA-1480 and CMSX-4 welds. However, further work is necessary to consider the coarsening kinetics.

**Thermodynamic and Kinetic Calculations**

The measured partitioning characteristics in welds suggest that the diffusional redistribution of elements between $\gamma$ and $\gamma'$ is affected by the weld cooling rate. The above hypothesis was evaluated with diffusion controlled growth calculations using DicTra. In these calculations the nucleation conditions are not considered. The $\gamma'$ was allowed to form at the boundary of $\gamma$ phase at a temperature where it was stable.

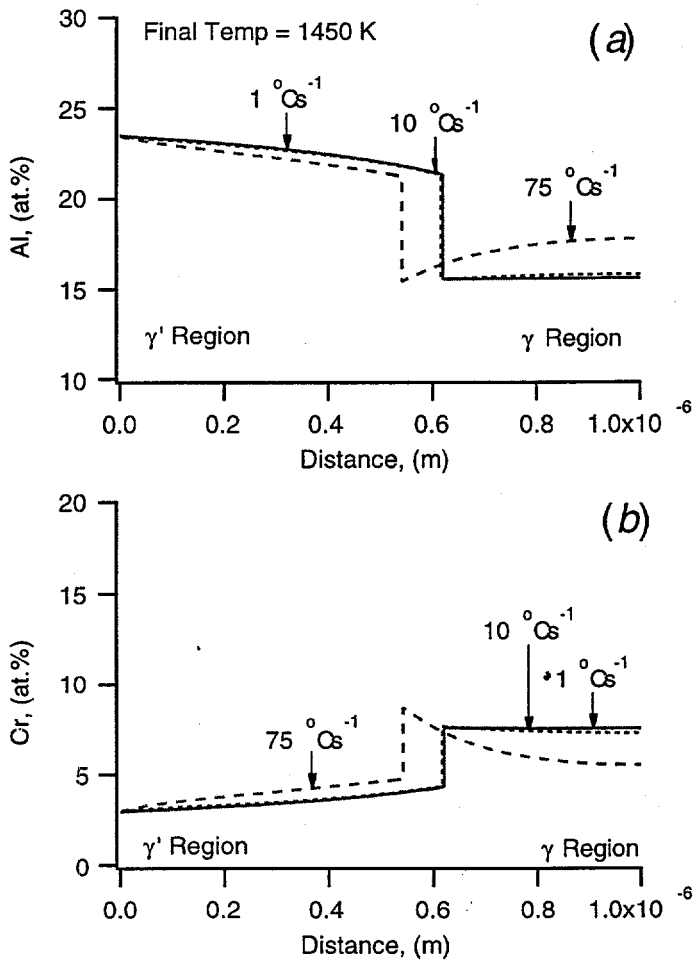


Fig. 9. Calculated concentration profiles across the $\gamma$ and $\gamma'$ phase regions at the end of simulation for different cooling rates. (*a*) aluminum, (*b*) chromium.

The calculated concentration profiles of Al and Cr in the $\gamma$ and $\gamma'$ phase for three different cooling rates are compared in Fig. 9 (*a*) & (*b*) respectively. At all cooling rates examined, the $\gamma'$ phase exhibited concentration gradients because the calculations did not consider diffusion in the $\gamma'$ phase. This is not consistent with the experimentally measured concentration profiles.

However, the concentration profiles within the $\gamma$ phase were similar to those measured by the atom probe. For cooling rate of 1 $°Cs^{-1}$, no significant concentration gradient was calculated. Calculations for 10 $°Cs^{-1}$ showed a small concentration gradient within the $\gamma$ phase. However, with calculations for 75 $°Cs^{-1}$, large Cr and Al concentration gradients were calculated in $\gamma$ phase. The calculations indicated that these concentration gradients develop at higher temperatures and are frozen-in by rapid cooling. The above result is quite consistent with the observed elemental partitioning in CMSX-4 and PWA-1480 welds. Note that for applying the calculations to the real PWA-1480 and CMSX-4 welds, one needs to consider the multicomponent partitioning and diffusion in the $\gamma'$ phase.

## Summary and Conclusions

Microstructure development and elemental partitioning between $\gamma$ and $\gamma'$ were measured in PWA-1480 electron beam welds and CMSX-4 pulsed-laser welds.

In PWA-1480 EB welds, eutectic $\gamma'$ phases were observed along the dendritic boundaries. The elemental partitioning between $\gamma$ and $\gamma'$ was found to be similar to that in PWA-1480 base metal.

In CMSX-4 pulsed laser welds, negligible eutectic $\gamma'$ was observed. In addition, fine and irregularly shaped $\gamma'$ precipitates were observed. The elemental partitioning between $\gamma$ and $\gamma'$ was found to be different from that measured in the base metal. Large concentration gradients were observed in the $\gamma$ phase.

The $\gamma'$ precipitation kinetics in CM247DS alloy was measured using dilatometry and showed differences with different cooling rates. The microstructural investigations showed that at large undercoolings the number density of $\gamma'$ precipitates increased and led to a finer size. This supports the microstructure development observations in PWA-1480 and CMSX-4 welds.

Thermodynamic and kinetic calculations for the Ni-Al-Cr alloy system showed that as the cooling rate increases, the $\gamma'$ growth leads to large concentration gradients in the $\gamma$ phase. The calculations agree with the atom probe results from PWA-1480 and CMSX-4 welds.

## Acknowledgments

The research was sponsored by the Division of Materials Sciences, U.S. Department of Energy, under contract DE-AC05-96OR22464 with Lockheed Martin Energy Research Corporation. The authors thank Drs. M. A. Burke and B. Seth of Westinghouse Electric Corporation for providing the CMSX-4 and CM247DS alloys used in this study. The authors also thank Mr. R. P. Schaefer of United Technologies Pratt and Whitney for providing PWA-1480 single crystal alloy. The authors acknowledge the technical assistance provided by R. W. Reed and K. F. Russell and Drs. B. Radhakrishnan and J. W. Cohron for helpful discussions. This research was conducted utilizing the Shared Research Equipment (SHaRe) User Program facilities at Oak Ridge National Laboratory.

## References

1. S. A. David, J. M. Vitek, S. S. Babu, L. A. Boatner, and R. W. Reed, *Sci. Tech. Weld. Joining*, **2**, 79-88 (1997).

2. J. M. Vitek, S. A. David, and L. A. Boatner, *Sci. Tech. Weld. Joining*, **2**, 109-118 (1997).

3. S. S. Babu, S. A. David, J. M. Vitek, and M. K. Miller, *J. de Physique IV.*, **6**, 253-258 (1996).

4. S. S. Babu, S. A. David, and J. M. Vitek, *Appl. Surf. Science*, **94/95**, 280-287 (1995).

5. B. Sundman, B. Jansson, and J.-O. Andersson,*Calphad*, **9**, 153-190 (1985).

6. N. Saunders, ThermoTech Ltd., Surrey Technology Center, Guildford, GU2 5YH, UK.

7. J.-O.Andersson, L. Höglund, B. Jönsson, and J. Ågren, *Fundamentals and Applications of Ternary Diffusion*, G. R. Purdy, ed., Pergamon Press, New York, NY, 1990, pp 153-163.

8. S. S. Babu, ORNL, Oak Ridge, TN 37831, Unpublished research (1998).

9. M. K. Miller, R. Jayaram, L.S. Lin and A. D. Cetel, *Appl. Surf. Science*, **76/77**, 172-176, (1994).

10. S. A. David, S. S. Babu, and J. M. Vitek, *Numerical Analysis of Weldability* H. Cerjack and H. K. D. H. Bhadeshia Eds. Institute of Materials, London, 1997, in press.

11. H. Murakami, H. Harada, H. K. D. H. Bhadeshia, *Appl. Surf. Science*, **76/77**, 177-183, (1994).

12. H. K. D. H. Bhadeshia, *J. de Physique*, **43**, C4-435 - 437, (1982).